Molecular Crystals and Liquid Crystals

Publication details, including instructions for authors and subscription information:
http://www.tandfonline.com/loi/gmcl20

Surface Energy Dissipation in Homeotropic Nematic Layers: The Role of Flexoelectricity and Surfactant Desorption

S. Ponti [a], G. Barbero [a], A. Strigazzi [a], Y. Marinov [b] & A. Petrov [a c]

[a] Dipartimento di Fisica, Instituto Nazionale di Fisica della Materia (INFM), Politecnico di Torino, Corso Duca degli Abruzzi 24, Corso Duca degli Abruzzi 24, Torino, Italy

[b] Institute of Solid State Physics, Bulgarian Academy of Sciences, 72 Tzarigradsko chaussee, 72 Tzarigradsko chaussee, Sofia, Bulgaria

[c] Institute of Solid State Physics, Bulgarian Academy of Sciences, 72 Tzarigradsko chaussee, Sofia, Sofia, Bulgaria

Version of record first published: 18 Oct 2010

Mol. Cryst. Liq. Cryst., Vol. 420, pp. 55–72, 2004

ISSN: 1542-1406 print/1563-5287 online
DOI: 10.1080/15421400490478164

Taylor & Francis
Taylor & Francis Group

SURFACE ENERGY DISSIPATION IN HOMEOTROPIC NEMATIC LAYERS: THE ROLE OF FLEXOELECTRICITY AND SURFACTANT DESORPTION

S. Ponti, G. Barbero, and A. Strigazzi
Dipartimento di Fisica and Instituto Nazionale di Fisica della Materia (INFM), Politecnico di Torino, Corso Duca degli Abruzzi 24, 10129 Torino, Italy

Y. Marinov
Institute of Solid State Physics, Bulgarian Academy of Sciences, 72 Tzarigradsko chaussee, 1784 Sofia, Bulgaria

*A. G. Petrov**
Dipartimento di Fisica and Instituto Nazionale di Fisica della Materia (INFM), Politecnico di Torino, Corso Duca degli Abruzzi 24, 10129 Torino, Italy; and Institute of Solid State Physics, Bulgarian Academy of Sciences, 72 Tzarigradsko chaussee, 1784 Sofia, Bulgaria

Homeotropic nematic layers of MBBA have been studied by a phase-sensitive flexoelectric spectroscopy method. They have been oriented by films of dilauroyl phosphatidyl choline (DLPC) and cetyl trimethyl-ammonium bromide (CTAB) self-assembled onto the cell glass plates. Using continuum theory, the transmitted light versus excitation frequency spectral shapes have been derived in terms of space variation of the nematic parameters (elastic constant, flexoelectric coefficient, rotational viscosity, and birefringence). These viscoelastic spectra contain information about the surface dissipation of the orientational energy for different aligning films that partially desorb from the surface and dissolve in the nematic, producing a gradient of the surfactant. A new type of flexoelectric effect dependent on the space derivative of flexo-coef-

Many thanks are due to N. V. Madhusudana, C. Oldano, and S. I. Torgova for useful discussions. This work has been supported by INCO-COPERNICUS (ERBIC15-CT96-0744) joint research project. A. G. Petrov gratefully acknowledges the support by INFM and by the Ministry of University and of Scientific and Technological Research of Italy (MURST) under the National Project "Cofinanziamento on Variational Problems." The authors are indebted to Dr. G. Minchev (ISSP-BAS) for the construction of a higher gain amplifier for the experimental setup.

*Corresponding author. E-mail: director@issp.bas.bg

ficients has been identified. This effect consists of a bulk flexo-torque source that substantially influences the apparent liquid crystal anchoring. Static and dynamic cases have been analyzed for a steplike surfactant distribution. Resulting spectra have been successfully compared with the experiment, yielding information about the surfactant gradient. These results provide new insights on the interfacial physics of nematic liquid crystals and solid surfaces, where flexoelectricity and desorption play a fundamental role.

Keywords: flexoelectricity; surfactant desorption; weak anchoring; surface viscosity

INTRODUCTION

The analysis of orientational surface viscosity effect reveals important dynamic aspects of the interaction between a nematic liquid crystal and a solid surface where orientational energy dissipation is involved. A new flexoelectric spectroscopy method has been used to investigate the temperature dependence of the surface viscosity of MBBA/CTAB interface. The method is based on a device for generation and amplification of flexo-electro-optic oscillations of light transmitted through a hometropic nematic layer [1,2]. Theoretically, the theory of flexoelectric spectroscopy for a non-desorbable surfactant layer was developed earlier [2,3], showing good agreement with the experiment in case of a nondesorbable cross-linked surfactant. However, it was noted [4] that the theory substantially deviates from the experiment in the case of excess surfactant in the aligning layer, which then desorbs away from the glass surface. Therefore, the aim of the present article is to theoretically analyse the effect of surfactant desorption and to compare the predicted spectra with the experimental ones.

In general, surfactant desorption looks like a problem to be carefully avoided rather than dealt with. However, in most practical situations it seems that this problem is unavoidable: even in the case of polymerizable surfactants, a certain percentage of nonpolymerized monomer can nevertheless redissolve from the surface into the bulk nematic. This process is even more important with ordinary surfactants, where the degree of desorption is simply controlled by the value of adsorption energy. Furthermore, desorbed surfactant molecules can be concentrated closer to the surfaces (being held in place by the surface electric field) rather than diffusing freely into the bulk, thus creating a subsurface nematic layer with modified material parameters by the presence of impurities. One has to remember that most experiments on homeotropic layers in the past were carried out with surfactants (e.g., lecithin) that readily desorb back into nematic (expressed, in particular, in the rapid depression of nematic clearing point just after cell assembly), although these experiments were ana-

lyzed by models of anchoring, without paying any attention to desorption. We shall see below that this is an important drawback and that such experiments need a careful reassessment, leading to re-evaluation of most anchoring parameters obtained.

MATERIALS AND METHODS

In the present work, we have measured first harmonic of the intensity of flexoelectrically modulated light, transmitted by a homeotropic nematic layer between crossed nicols, subjected to a dc + ac electric field parallel to the layer substrates [1,2], following a slow frequency sweep, provided by a computer-interfaced lock-in amplifier (SR830).

Methoxybenzilidene butylaniline (MBBA) from Reachim, Russia ($T_c = 43$°C) was used throughout. The nematic material was sandwiched between two glass substrates with homeotropic treatment. This treatment involved deposition of self-assembled multilayers from synthetic lecithin dilauroyl phosphatidyl choline (DLPC; Fluka, Germany). DLPC was dissolved in chloroform, and lipid concentration was varied in the range 1–100 mM in order to vary the multilayer thickness [5]. Glass plates were dipped in solution for 20 min and then air dried at 50°C. For comparison, cetyl trimethyl-ammonium bromide (CTAB) monolayers and cross-linked films of silanes were used for orientation. The CTAB monolayer films were self-assembled by dipping the precleaned glass plates into water solutions of the surfactant CTAB (Merck, Germany 99% p.a) at 1.6×10^{-5} M concentration in bidistilled water for 10 min. The plates were then withdrawn with two different speeds (i.e., 0.6 cm/min and 2 cm/min) to obtain densely packed and loosely packed orienting monolayers for MBBA homeotropic alignment [2,6]. For comparison, cross-linked orienting films of silanes were also employed as follows: 0.1 vol% of ODS-E (Chisso, Japan) was dissolved in 9:1 isopropyl alcohol/water, and glass plates were dipped in the solution for several hours under continuous stirring. The plates were then rinsed with distilled water and ODS-E was polymerized, keeping it at 110°C for 1 h.

Liquid crystal cells were then assembled using 100 μm thick Cu-foil spacers serving as electrodes, providing an in-plane field. The samples were sealed by Araldite (epoxy-glue). The interelectrode distance was 2 mm. The electric field can be smoothly nonhomogeneous at the cell surface because of the fringing effect. A dependence of the field from the in-plane position at the surface can be expected. The transmitted light intensity is an average of all surface values within the spot interrogated by the laser beam. In our case only the central area (about 1 mm for diameter) of the cell surface was interrogated. For symmetry reasons the in-plane nonhomogeneity of the field averages to zero in such region.

The cells were placed in a Mettler FP82 heating stage for measurements at different temperatures. One day after filling the cell, the MBBA clearing point was found to drop down to 40°C: this is evidence for the desorption of the DLPC surfactant films. An electric field parallel to the cell plates directed at 45° with respect to crossed polarizers was applied to the nematic cell by means of the copper spacers. The frequency dependence of the transmitted light modulation was obtained by means of a flexoelectric spectrometer in the range (5–2000) Hz.

THEORY

Fundamental Equations for Space-Variable Material Parameters and Static Solutions

Let us consider a medium in which a desorption of the surfactant from the cell plates takes place: after desorption, the surfactant dissolves in the liquid crystal. This implies two steps: desorption and diffusion. Although desorption time has not been directly measured, the second step seems much more rapid than the first. The diffusion time for the cell is given by $\tau = d^2/D$, where d is the cell thickness and D the diffusion coefficient. It can be estimated $\tau \sim 25\,\mathrm{s}$ for the whole cell thickness, with $D \sim 4.10^{-6}\mathrm{cm}^2\,\mathrm{s}^{-1}$ [7] and $d = 100\,\mu\mathrm{m}$. However, since our cells perform well for a few days without changing their electrooptic response, we should expect a spatially inhomogeneous equilibrium distribution of surfactant despite fast diffusion.

Thus, the physical situation we imagine is the following. The desorption takes place as the sample is filled with the liquid crystal. The desorbed lecithin, due to diffusion, enters immediately into the liquid crystal bulk. However, it can not diffuse far enough, being attracted by a surface electric field (due to the selective ions adsorption, always present in the liquid crystal cell), decreasing in a quasi exponential manner and vanishing in the bulk over a few Debye screening lengths [8,9]. Since the dipolar moment of the lecithin molecules is rather large (∼30D), the dielectric coupling between the surface electric field and the lecithin dipoles gives rise to a nonhomogeneous distribution of lecithin molecules. They are spatially distributed according to the Maxwell-Boltzmann statistics $n(z) = n_0 \exp[-U(z)/k_B T]$, where n_0 is the bulk density of lecithin molecules, k_B the Boltzmann constant, T the temperature, and the electrostatic energy of the dipoles is $U(z) = -\vec{p}.\vec{E}(z)$. $\vec{p}$ is the dipolar moment of the lecithin molecule, and $\vec{E}(z)$ the effective electric field localized near the surface. The same equation also describes the behavior of the nematic liquid crystal (NLC) molecules but with different values of $\vec{p}$. Since $\vec{p}$ of lecithin is much larger than that of liquid crystal (LC) molecules, an increase of the lecithin

concentration near the surface is expected. By assuming for the adsorption field, in the semi-infinite approximation, the expression $\vec{\mathrm{E}} = \mathrm{E}(z)\hat{z} = \mathrm{E}_0 \exp(-\mathrm{z}/\lambda_D)\hat{z}$, where λ_D is the Debye screening length, E_0 the surface field, and $\hat{z}$ the unit vector normal to the glass plates, we have $U(z) = -p\mathrm{E}_0 \exp(-\mathrm{z}/\lambda_D)$ in the hypothesis that the lecithin dipoles are homeotropically oriented as the LC director. Since λ_D for MBBA is of the order of 1 μm [10], E(z) is localized over (1–2) μm. We suppose that the surface electric field due to the adsorption can be considered independent of the applied voltage, and thus a true surface property of the lecithin-liquid crystal interface. As a consequence, the gradient can be considered practically time independent during each measurement run (which covers almost 1 h).

The surfactant contains strongly asymmetric molecules: then it contributes to the effective elastic, viscous, flexoelectric, and optical properties of the resulting LC phase. Consequently, a spatial dependence of the material parameters has to be considered [11–14].

In the discussion reported above, the surface field is due to a selective adsorption of ions. Another source of the field can be the discrete distribution of the lecithin dipoles on the glass, which also creates a surface field exponentially decreasing in the LC bulk. The surface polarized layer is due to the strong difference in chemical affinity with the glass of the alkyl and zwitterionic parts of the lecithin molecule. In fact, the two alkyl tails are hydrophobic, whereas the zwitterion is hydrophilic, as is the glass plate. In this case, the typical surface field penetration length is comparable with the average distance between discrete surface dipoles [19].

We treat the homeotropic cells filled by MBBA in the low field approximation. The general equation governing the balance of the elastic, flexoelectric, and viscous torques changing in time in the small-angle approximation is obtained by means of a functional derivative of the total free energy and of the sample dissipation function [15]. Standard calculations give

$$k(z)\frac{\partial^2\theta}{\partial z^2} + \frac{dk}{dz}\frac{\partial\theta}{\partial z} - \frac{de(z)}{dz}E(t) = \gamma(z)\frac{\partial\theta}{\partial t}, \tag{1}$$

where $k(z)$ is the bend elastic constant, $e(z)$ is the bend flexoelectric coefficient, and $\gamma(z)$ is the bulk viscosity. $\theta(z,t)$ is the tilt angle made by the nematic director with respect to the z axis, normal to the cell plates, and $E(t) = E_1\cos(\omega t)$ is the external ac electric field. In Equation (1) the second and third terms originate from the spatial inhomogeneities of the liquid crystal due to the desorption of the surfactant controlled by the surface field due to the adsorption of ions. The third term represents a new type of gradient flexoelectric effect that gives rise to a bulk torque

proportional to the gradient of flexoelectric coefficient. In Equation (1) the dielectric contribution has been neglected since the tilt angle θ is very small at the threshold, and this term is second order in θ, whereas the flexoelectric source of the distortion is linear in θ. In fact, in the case of small distortions the ratio between the flexoelectric ($eE\theta/\lambda$) and the dielectric ($\varepsilon_0\varepsilon E^2\theta$) torque turns out to be of the order of 10^3.

Since we are interested in the flexoelectric response of the system, our experimental setup is sensitive to the first harmonic in Equation (1). The left-hand side of Equation (1) represents the bulk density of the elastic and flexoelectric torque, whereas the right-hand side is the bulk density of the viscous torque. We emphasize that the space derivative of the flexoelectric coefficient is responsible for a new type of flexoelectric effect, acting as a bulk source of torque. In writing Equation (1) we have neglected the contribution coming from the spatial derivative of the electric field (which in principle is different from zero due to the fringing effect) because it is of the kind $e(dE/dz) \sim eEd/a^2$, where d and a are the cell thickness and the electrode distance, respectively. This term has to be compared with $(de/dz)E \sim eE/\lambda$, where λ is a convenient thickness of the surface layer of the order of a few Debye lengths λ_D, along which the LC parameters essentially change. In our case, with $d \sim 100\,\mu\text{m}$, $a \sim 2\,\text{mm}$, and $\lambda \leq d$, the fringing contribution is negligible with respect to the other. In this framework the related boundary conditions are [16]

$$\pm k(z)\frac{\partial\theta}{\partial z} \mp e(z)E(t) + W\theta = \chi\frac{\partial\theta}{\partial t}, \quad z = \pm d/2, \tag{2}$$

where W is the anchoring strength at the surfaces of the sample and χ is the surface viscosity (measured as bulk viscosity times length). In order to solve Equation (1) with space-dependent coefficients, the straightforward way is to subdivide the cell thickness d in m regions of thickness d/m, each of them characterized by constant parameters. In writing the equations system, convenient continuity conditions must be considered. As a consequence, the analytical computation becomes impossible. In order to show the interdependence of the various parameters characterizing the phenomenon, we decided to solve the problem applying a two-groups approximation. Then the cell turns out to be subdivided into three regions: two regions of thickness λ close to the glass plates (surface layers), and the remainder part of the cell of thickness $d - 2\lambda$ (bulk). The thickness λ plays the role of a penetration length, dividing the cell into a surface part, where the parameters are strictly dominated by the distribution of lecithin molecules confined by the surface field, and in a bulk part where the parameters are essentially determined by the original liquid crystalline material. The length $\lambda \ll d$ enters in the system equations as a fit parameter for describing only the low frequency behavior, as will be shown later.

We will assume that the material properties have different but spatially constant values in the surface layer and in the bulk. We indicate with the subscripts S and B the physical parameters of the LC in the surface layer and in the bulk, respectively. The balance of the torques has to be studied in both regions. It yields the following diffusion-like equations:

$$\begin{gathered} k_S \frac{\partial^2 \theta_S}{\partial z^2} = \gamma_S \frac{\partial \theta_S}{\partial t}, \quad \text{for} - d/2 < z < -d/2 + \lambda \quad \text{and} \quad d/2 - \lambda < z < d/2, \\ k_B \frac{\partial^2 \theta_B}{\partial z^2} = \gamma_B \frac{\partial \theta_B}{\partial t}, \quad \text{for} \quad -d/2 + \lambda < z < d/2 - \lambda, \end{gathered} \tag{3}$$

with interfacial conditions over the surface-bulk interface

$$k_S \frac{\partial \theta_S}{\partial z} - e_S E(t) = k_B \frac{\partial \theta_B}{\partial t} - e_B E(t), \quad \text{for} \quad z = \pm d/2 \mp \lambda, \tag{4}$$

and boundary conditions

$$\pm k_S \frac{\partial \theta_S}{\partial z} \mp e_S E + W \theta_S = \chi \frac{\partial \theta_S}{\partial t}, \quad \text{for} \quad z = \pm d/2. \tag{5}$$

Since experiments have been performed with a dc+ac electric field $E = E_0(1 - \cos \omega t)$ (in order to bias the optical system from zero transmission), the torque balance equations have to be solved in both static and dynamic regime. The very simple case of the static regime already gives interesting information: the spatial variation of the optical anisotropy $\Delta n(z)$, of the elastic constant $k(z)$, and of the flexoelectric coefficient $e(z)$ contribute to the detectable anchoring energy, renormalizing it by a factor proportional to the difference between subsurface and bulk values of these physical properties (see Appendix A).

Dynamic Solutions

Let us consider the case of an ac electric field applied to the sample. As mentioned above, we limit our analysis to the first harmonic since the flexoelectric effect is linear and the distortion is small. The differential Equations (3) admit solutions of the kind

$$\theta_{S,B} = \Theta^+_{S,B} e^{i\omega t} \sinh\left[(1+i)\frac{z}{\xi_{S,B}}\right] + \Theta^-_{S,B} e^{-i\omega t} \sinh\left[(1-i)\frac{z}{\xi_{S,B}}\right], \tag{6}$$

where the penetration lengths

$$\xi_{S,B} = \sqrt{\frac{2k_{S,B}}{\omega \gamma_{S,B}}}, \tag{7}$$

are frequency dependent. The integration constants $\Theta_{S,B}^{+,-}$ have to be calculated by imposing the boundary and the interface conditions, respectively. The integration constants turn out to be

$$\Theta_S^{\pm} = \frac{e_S E_0}{2k_S} \frac{1}{\left[\frac{1\pm i}{\xi_S}\coth[(1\pm i)\delta_S] \mp \frac{\chi}{k_S} i\omega + \frac{1}{b}\right]\sinh[(1\pm i)\delta_S]},$$
$$\Theta_B^{\pm} = \frac{E_0}{2}\left(\frac{e_B - e_S}{k_B}\right)\frac{\xi_B}{(1\pm i)\cosh[(1+i)\ell_B]} + \Theta_S^{\pm}\frac{\xi_B}{\xi_S}\frac{k_S}{k_B}\frac{\cosh[(1\pm i)\ell_S]}{\cosh[(1\pm i)\ell_B]}, \tag{8}$$

where $\delta_S = d/(2\xi_S)$ and $\ell_{B,S} = (d/2 - \lambda)/\xi_{B,S}$.
The transmitted light intensity in the approximation of small distortion is given by

$$I(t) = I_0 \sin^2\left(\frac{\Delta\varphi}{2}\right), \tag{9}$$

where $\Delta\varphi = 2\pi\Delta L/\lambda_0$ is the phase difference, λ_0 being the light wavelength and ΔL the optical path difference between the ordinary and extraordinary components. In Equation (9) I_0 is the impinging laser light intensity.

In the case of small $\Delta\varphi$, using the analysis reported in Appendix B, $I(t)$ can be written as

$$I(t) \approx I_0\left(\frac{2\pi}{\lambda_0}\right)^2 \Delta n_B \langle\theta_{0,B}^2\rangle[\langle\theta_{0,B}\theta_{1,B}\rangle\Delta n_B + \frac{2\lambda}{d}\langle\theta_{0,S}\theta 1, S\rangle\Delta n_s]d^2, \tag{10}$$

where θ_0 stands for the static solution and θ_1 for the dynamic one, and $\langle\ldots\rangle$ denotes the averaging over the corresponding B and S regions. In the derivation of Equation (10) the time-independent terms θ_0 are omitted, as well as the time-dependent terms of second power in θ_1, because they give rise to the second harmonic in the light intensity. Moreover, terms proportional to $\langle\theta_{0,S}^2\rangle = 0(\lambda/d)$ are neglected. The complex expressions of the integrals appearing in Equation (10) are reduced to a real form (see Appendix B). However, unlike the boundary conditions, Equation (10) already contains both an in-phase component ($\cos\omega t$) and a quadrature component ($\sin\omega t$). Since the expected value of λ is a few μm, and already at 1 Hz $\xi \sim 5\,\mu$m while $d = 100\,\mu$m, the approximation $\sinh[(1\pm i)\ell_S]/\sinh[(1\pm i)\delta_S] \approx \exp[-\lambda(1\pm i)/\xi_S]$ is used. In this way we get

$$\frac{I(t)}{I_0} = X(\omega)\cos(\omega t) + Y(\omega)\sin(\omega t) = R(\omega)\cos(\omega t - \psi(\omega)), \tag{11}$$

where $R(\omega) = \sqrt{X^2 + Y^2}$ and $\tan\psi = Y/X$. The in-phase $X(\omega)$ and the quadrature $Y(\omega)$ components of the light intensity are reported in the Appendix B, Equations (B 12–B 15). It must be stressed that both $X(\omega)$ and $Y(\omega)$ components contain an exponential term of the type $\exp(-\lambda/\xi_S)$, which is important at lower frequencies.

The expression of $R(\omega)$ can be simplified, taking into account that λ and ξ are expected to be of the order of few μm: then in expressions of the type $(d/2 - \xi - \lambda)$, both ξ and λ were neglected with respect to d. Finally, the exponential terms in X and Y could safely be neglected above 10 HZ, see Equation (7). Then the first harmonic amplitude of the light intensity can be written as

$$R(\omega) = \frac{1}{\omega}\sqrt{P_1^2 + 2P_2\frac{P_2 + P_1(2 - P_3\sqrt{\omega})}{1 + (1 - P_3\sqrt{\omega})^2}}, \tag{12}$$

where $P_{1,2,3}$ are the material parameters defined as

$$\begin{aligned} P_1 &= 2\left(1 - \frac{e_S}{e_B}\right)\frac{k_B}{\gamma_B}C, \\ P_2 &= 2\frac{\Delta n_s}{\Delta n_B}\left[\frac{e_S}{e_B}\frac{k_B}{k_S}\right]^2\left(\frac{1}{1 + (1 - e_S/e_B)d/2b}\right)\frac{k_S}{\gamma_S}C, \\ P_3 &= \chi\sqrt{\frac{2}{k_S\gamma_S}} \end{aligned} \tag{13}$$

where $b = k_S/W$ and

$$C = \frac{1}{6}\left(\frac{\pi}{\lambda_0}\right)^2\Delta n_B^2\left(\frac{e_B}{k_B}\right)^4 E_0^4 d^4\left[\frac{1 + (1 - e_s/e_B)d/2b}{1 + d/2b}\right]^3. \tag{14}$$

P_1, P_2, and P_3 are measured in s^{-1}, s^{-1}, and $\sqrt{s}$, respectively, since $R(\omega)$ is a dimensionless quantity.

EXPERIMENTAL RESULTS AND DISCUSSION

The experimental data concerning the first harmonic modulation spectra of MBBA cell with DLPC aligning film are reported in Figure 1 at three different temperatures (25°C, 30°C, and 35°C), together with the best three parametric fit curves related to the present theory. In Figure 2 the reduced function $\omega R(\omega)$ is reported for $T = 25$°C (Figure 2(a)), for $T = 30$°C (Figure 2(b)), and for $T = 35$°C (Figure 2(c)), together with the best-fit curves according to the present desorption theory, three parametric (curve 2) and five parametric (curve 3) fits.

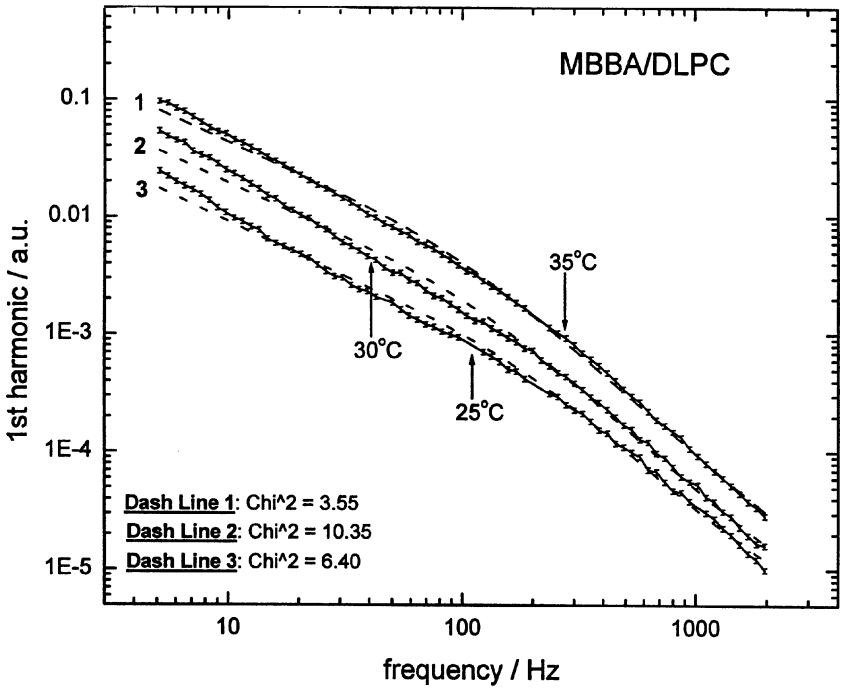

FIGURE 1 Frequency dependence of the first harmonic $R(\omega)$ of flexoelectrically modulated transmitted light through a homeotropic nematic layer of MBBA at different temperatures. The homeotropic orientation was achieved by self-assembled DLPC layers (by dipping the substrates in chloroform solution of DLPC, bulk concentration 0.3 mM). The layer thickness is 100 μm, the electrode distance is 2 mm, the ac voltage is 40 V_{pp}, the dc bias is 20 V. Experimental data and relevant fits (solid and dashed lines, respectively) are presented at 25°C, at 30°C, and at 35°C. The parameters are: for $T = 25$°C, $P_1 = 0.159$, $P_2 = 0.355$, and $P_3 = 0.041$; for $T = 30$°C, $P_1 = 0.194$, $P_2 = 0.842$, and $P_3 = 0.054$; for $T = 35$°C, $P_1 = 0.283$, $P_2 = 1.942$, and $P_3 = 0.061$.

Let us compare these results with the ones already reported in Marinov *et al.* [2], which are relevant to the first harmonic flexoelectric spectra of MBBA anchored on a not-dense CTAB monolayer at different temperatures in the nematic range. Since the CTAB molecules have a very high adsorption energy with respect to hydrophilic glass plates, the desorption phenomenon was practically absent. Thus the shape of $R(\omega)$ closely followed the theoretical predictions: in the lower frequency region $R \propto \omega^{-1}$, and in the higher frequency region $R \propto \omega^{-3/2}$. This can be recovered by Equation (12) in the case of $P_1 \equiv 0$, which means $e_B = e_S$ (see Equation (13)), as in the absence of desorption. In other words, Equation (12) reduces for $P_1 = 0$ to the one

derived in Petrov *et al.* [1] and Marinov *et al.* [2], where desorption phenomenon was not taken into account. In our case, from Equation (12) we obtain in the low frequency range ($\omega \to 0$)

$$R(\omega) \approx \frac{|P_1 + P_2|}{\omega}, \tag{15}$$

whereas in the high frequency range ($\omega \to \infty$) Equation (12) reads

$$R(\omega) \approx \frac{|P_1|}{\omega}. \tag{16}$$

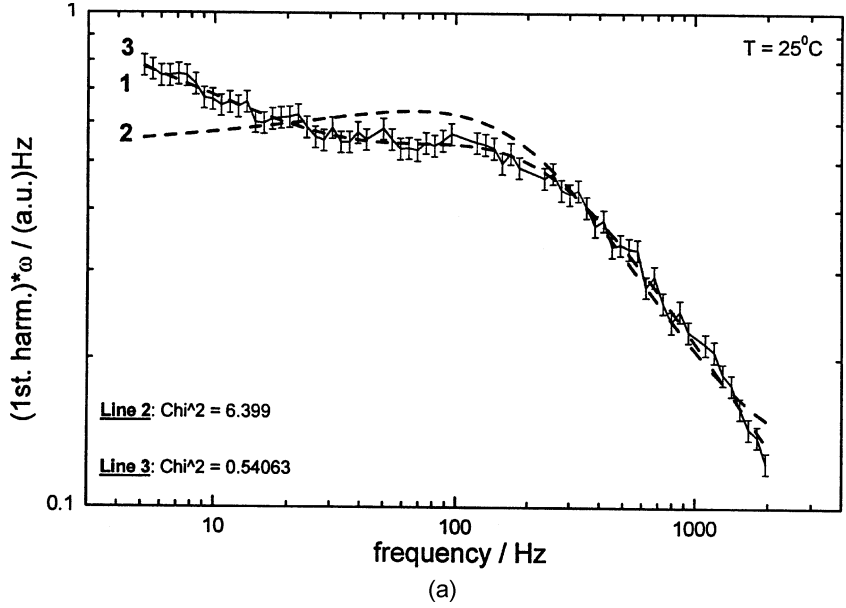

FIGURE 2 Best fit of the renormalized spectra $\omega R(\omega)$. Figure 2(a) corresponds to $T = 25$°C, (b) to $T = 30$°C and (c) to $T = 35$°C. (1) Experimental curve with estimated uncertainties of the order of 5%, due to the instrumental accuracy. (2) 3-parameter fit accounting for the surfactant gradient (present theory). Best fit parameters are the same as in Figure 1. (3) Best fit (dash line) of the renormalized spectra $\omega R(\omega)$, considering in $R(\omega)$ the exponential contribution $P_4 \exp(-P_5\sqrt{\omega})$. P_4 is a complicated function of the material parameters, and P_5 is simply given by $\lambda\sqrt{2\gamma_S/k_S}$. Best fit parameters: Figure 2(a) for $T = 25$°C, $P_4 = 1.338$ and $P_5 = 0.209$; (b) for $T = 30$°C, $P_4 = 6.276$ and $P_5 = 0.166$; (c) for $T = 35$°C, $P_4 = 11.259$ and $P_5 = 0.061$. By assuming $\gamma_S/k_S \sim \gamma_B/k_B$, the corresponding surface layer thickness are given by: $\lambda = 1.4\,\mu$m (25°C), $\lambda = 1.3\,\mu$m (30°C), and $\lambda = 0.5\,\mu$m (35°C).

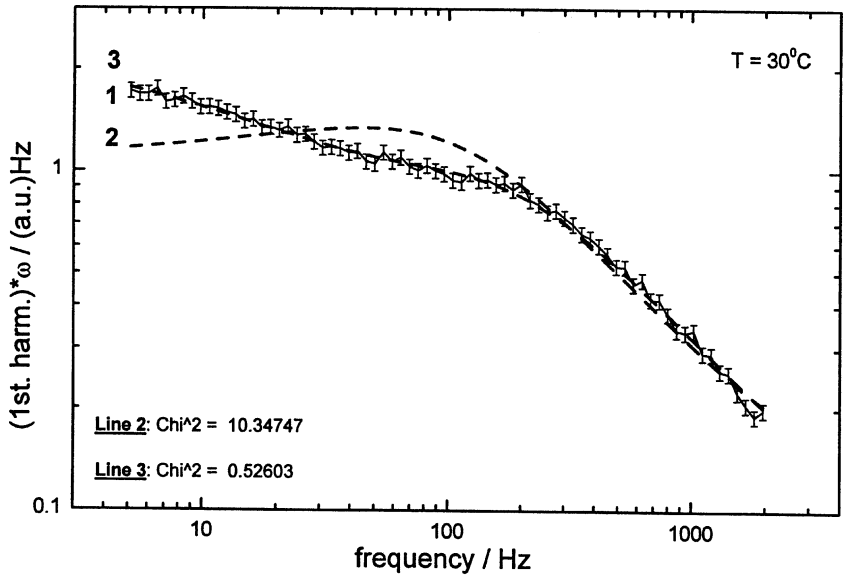

(b)

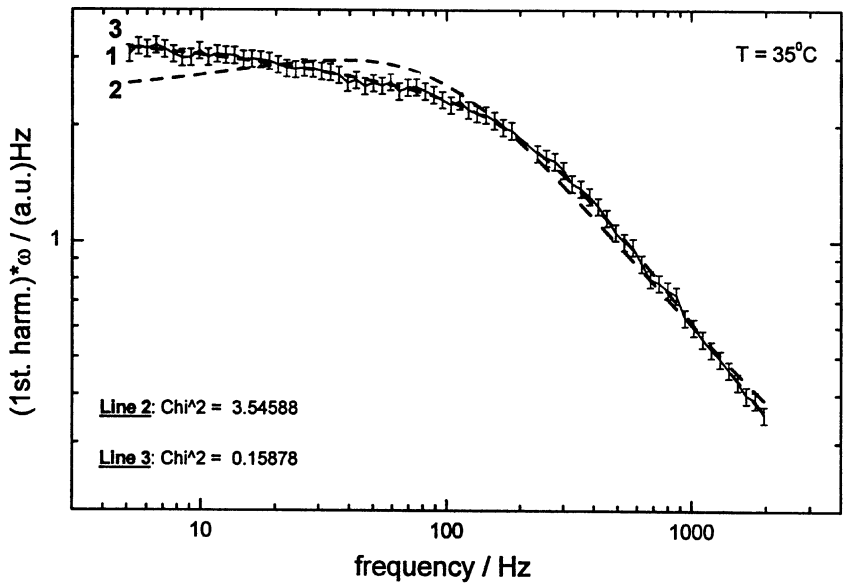

(c)

FIGURE 2 Continued.

Just the first part of the second asymptotic behavior can be explored by our experimental setup. We will analyze the experimental data by means of Equation (12) valid in the frequency range $5 \leq \nu \leq 2 \times 10^3$ Hz. In comparison with the loosely covered glass plates, a middle frequency "plateau" appeared on the spectral curves of dense CTAB, not explainable by the previous theory [4]. This interesting phenomenon is much more softly, also with orienting (multi)layers of synthetic lecithin (DLPC) self-assembled by dipping glass plates in chloroform solution (Figure 1).

Systematic fits of the spectra obtained with MBBA/DLPC at different temperatures have been performed based on the 3-parametric expression, Equation (12). Figure 1 demonstrates that the fit captures the essential features of the curves. Fitting parameters at $T = 25°\text{C}$ are $P_1 = 0.159$, $P_2 = 0.355$, and $P_3 = 0.041$; at $T = 30°\text{C}$ they are $P_1 = 0.194$; $P_2 = 0.842$, and $P_3 = 0.054$; and at $T = 35°\text{C}$ they are $P_1 = 0.283$, $P_2 = 1.942$ and $P_3 = 0.061$. The stability and the sensitivity of the best fitting procedure have been tested. Figure 2, obtained by renormalizing the spectrum for the overall ω^{-1} slope, clearly shows that the previous theory (curve 2) is able to fit only the very high frequency region of the spectrum in terms of surface viscosity, but it substantially deviates from the experiment in the central and low frequency regions. On the other hand, the present theory (curve 3) provides a reasonable fit over the whole frequency range. The comparison of the Chi^2 tests for 3-parametric and 5-parametric fits shows the supremacy of the new extended theory (i.e., Chi^2 < 1; see Figure 2). According to our experimental data, $P_1 > 0$. This implies taking into account the first equation of the system in Equation (13), that both $(1 - e_S/e_B) > 0$ and $C > 0$. Consequently, $e_s < e_B$, which could be explained by a dilution of the quadrupolar electric anisotropy of the nematic by the presence of lecithin.

To explain the systematic deviation in the lower frequency region we have to take into account that in the expression of the light intensity, Equation (11), the exponential term cannot be neglected (see Appendix B, the exponential contributions E_X and E_Y in Equations (B 14) and (B 15)). In the lower frequency range such contributions are proportional to

$$\frac{1}{\omega}\exp\left(-\lambda\sqrt{\frac{\gamma_S}{2k_S}}\sqrt{\omega}\right).$$

It follows that in this frequency range the first harmonic amplitude of the light intensity given by Equation (12) also contains under the square root a term proportional to $\exp(-\lambda\sqrt{2\omega\gamma_s/k_s})$; the phenomenon depends here on the surface layer thickness λ.

By fitting the experimental data in the low frequency range by an additional exponential term of a general form $P_4 \exp(-P_5\sqrt{\omega})$, where P_4 is a complicated function of the material parameters and $P_5 = \lambda\sqrt{\frac{2\gamma_s}{k_s}}$, and

assuming $\gamma_s/k_s \sim \gamma_s/k_B$, we can finally obtain $\lambda \sim 1.4\,\mu m$ at $T = 25°C$, $\lambda \sim 1.3\,\mu m$ at $T = 30°C$, and $\lambda \sim 0.5\,\mu m$ at $T = 35°C$, (see Figure 2). These values for the surface layer thickness are comparable to the Debye screening length [10], as expected. The quality of these 5-parametric fits is much better now (curves 3 on Figures 3(a)–3(c), and all the details of the renormalized spectra are reliably reproduced.

Although a convincing fit needs a relatively large number of parameters, we demonstrate the physical origin of any one of these parameters and how they come into play when extending the spectral region to still lower frequencies. The nonzero values of the last two parameters of the exponential term could be considered a direct proof of the existence of subsurface regions of nonzero thickness with modified properties.

CONCLUSIONS

Experimental results on the surface dissipation of orientational energy in homeotropic nematics demonstrated a good agreement with the simple theory only in the case of a minor amount of surfactant or a cross-linked orienting layer on the glass plates but a disagreement in the case of excess of monomeric surfactant (DLPC). The idea that the disagreement can be due to the monomer desorption and to the buildup of a surfactant gradient near the cell walls is tested here. A nontrivial extension of the existing theory by including space variations of material parameters close to the surface has been done, taking into account the spatial gradients in the surfactant concentration. A comparison with the experiments reveals the importance of these gradient contributions and the existence of a new type of bulk flexoelectric torque due to the spatial variation of the flexoelectric coefficient. It is stressed that desorption of surfactants is a common situation in most practical cases of homeotropic layers, and it is indispensable to cosider it, if reliable data of surface parameters are being looked for.

REFERENCES

[1] Petrov, A. G., Ionescu, A. Th., Versace, C., & Scaramuzza, N. (1995). *Liq. Cryst.*, *19*, 169.
[2] Maarinov, Y., Shonova, N., Versace, C., & Petrov, A. G. (1999). *Mol. Cryst. Liq. Cryst.*, *329*, 1145.
[3] Derzhanski, A. & Petrov, A. G. (1979). *Acta Physica Polonica*, *A55*, 747.
[4] Marinov, Y., Shonova, N., Naydenova, S., & Petrov, A. G. (2000). *Mol. Cryst. Liq Cryst.*, *351*, 411.
[5] Proust, J. E., Ter-Minassian-Saraga, L., & Guyon, E. (1972). *Solid State Commun.*, *11*, 1227.
[6] Naydenova, S., Petrov, A. G., & Yarwood, J. (1995). *Langmuir*, *11*, 3435.
[7] de Gennes, P. G. & Prost, J. (1995). *The Physics of Liquid Crystals* (Oxford: Oxford Univ. Press).

[8] Israelachvili, J. 1998. *Intermolecular & Surface Forces*, 2nd ed. (London: Harcourt Brace and Company), Chap. 12, p. 215.
[9] Ponti, S., Ziherl, P., Ferrero, C., & Žumer, S. (1999). *Liq. Cryst.*, *19*, 1171.
[10] Thurston, N. R., Cheng, J., Meyer, R. B., & Boyd, G. D. (1984). *J. Appl. Phys.*, *56*, 264.
[11] Alexe-Ionescu, A. L., Barbero, G., & Ponti, S. (1996). *Liq. Cryst.*, *20*, 17.
[12] (a) Nehring, J. & Saupe, A. (1971). *J. Chem. Phys.*, *54*, 337.
(b) Nehring, J. & Saupe, A. (1972). *J. Chem. Phys.*, *56*, 5527.
[13] Vertogen, G. (1983). *Physica A*, *117*, 227.
[14] Prost, J. & Marcerou, J. P. (1977). *J. de Phys. Paris*, *38*, 315.
[15] Goldstein, H. *Classical Mechanics* 1st ed. New York: Addison-Wesley, Chap. 2, p. 22.
[16] Elsgolts, L. (1980). *Differential Equations and the Calculus of Variation*, 1st ed. Moscow: (Mir). Chap. 7, p. 341.
[17] Schmidt, D., Schadt, M., & Helfrich, W. (1972). *Naturforsch.*, *27a*, 277.
[18] Blinov, L. M., Kabayenkov, A. Yu, & Sonin, A. A. (1989). *Liq. Cryst. 5*, 645.
[19] Barbero, G. & Petrov, A. G. (1994). *J. Phys.: Condens. Matter*, *6*, 2291.

APPENDIX A. STATIC SOLUTION: TORQUE BALANCE AND ANCHORING

As is well known, the dielectric coupling of a transverse electric field with MBBA nematic director stabilizes the initial configuration due to the negative dielectric anisotropy. Thus, in considering the flexoelectric bending we are allowed to neglect the dielectric contribution, which is of the second order which respect to the deformation and competes with the flexoelectric linear coupling, reducing the distortion itself [18].

Then the torque balance in the presence of a dc electric field becomes

$$\begin{aligned} k_S \frac{d^2\theta_S}{dz^2} &= 0, \quad \text{for} \quad -d/2 < z < -d/2 + \lambda \quad \text{and} \quad d/2 - \lambda < z < d/2, \\ k_B \frac{d^2\theta_B}{dz^2} &= 0, \quad \text{for} \quad -d/2 + \lambda < z < d/2 - \lambda \end{aligned} \tag{A1}$$

the correspondent boundary conditions are

$$\pm k_S \frac{d\theta_S}{dz} + W\theta_S = \pm e_S E_0, \quad \text{for} \quad z = \pm d/2, \tag{A2}$$

and the interface conditions for torque continuity are

$$k_S \frac{d\theta_S}{dz} - e_S E_0 = k_B \frac{d\theta_B}{dz} - e_B E_0, \quad \text{for} \quad z = \pm d/2 \mp \lambda \tag{A3}$$

The solutions of the equilibrium equations are

$$\begin{aligned} \theta_S &= A_S z, -d/2 < z < -d/2 + \lambda \quad \text{and} \quad d/2 - \lambda < z < d/2, \\ \theta_B &= A_B z, -d/2 + \lambda < z < d/2 - \lambda, \end{aligned} \tag{A4}$$

where

$$A_S = \frac{e_S}{k_S(1+d/2b)}E_0,$$
$$A_B = \frac{e_B-(e_S-e_B)d/2b}{k_B(1+d/2b)}E_0, \tag{A5}$$

and $b = k_S/W$. Now, we calculate the experimentally measurable optical path difference ΔL between the ordinary and extraordinary components passing through the LC layer placed between crossed polarizers, defined by

$$\Delta L = \int_{-d/2}^{d/2} \Delta n(z)\theta^2(z)dz. \tag{A6}$$

Using Equations (A4) and (A5) for $\theta(z)$, we obtain

$$\Delta L = \frac{\Delta n_B e_B^2}{12k_B^2}\frac{E_0^2 d^3}{(1+d/2b)^2}\left\{N+\left[\left(1-\left(\frac{e_S}{e_B}-1\right)\frac{d}{2b}\right)^2-N\right]\left(1-\frac{2\lambda}{d}\right)^3\right\}, \tag{A7}$$

where

$$N = \frac{\Delta n_S}{\Delta n_B}\frac{e_S^2}{e_B^2}\frac{k_B^2}{k_S^2}. \tag{A8}$$

This result has an important implication: if the experimentalist is not aware of the bulk source of flexoelectric torque, he would like to interpret the above $\Delta L(d)$ dependence in terms of an "apparent" anchoring,

$$\Delta L = \frac{\Delta n_B e_B^2}{12k_B^2}\frac{E_0^2 d^3}{(1+d/2b_{app})^2}. \tag{A9}$$

However, we have shown above that

$$(1+d/2b_{app})^{-2} = (1+d/2b)^{-2}\left\{N+\left[\left(1-\left(\frac{e_s}{e_B}-1\right)\frac{d}{2b}\right)^2-N\right]\left(1-\frac{2\lambda}{d}\right)^3\right\}, \tag{A10}$$

If the anchoring energy is very small, i.e., of the order of 10^{-4} ert/cm^2 [17], Equation (A10) can be rewritten as

$$(1+d/2b_{app})^{-2} = (1+d/2b)^{-2}\left[1+6(N-1)\frac{\lambda}{d}-2\zeta\right], \tag{A11}$$

where $\zeta = [(e_S - e_B)/e_B](d/2b) << 1$.. This expression shows that the spatial variations of Δn, k, and e contribute to the detectable anchoring energy. By assuming that ζ is negligibly small, from Equation (A11) it is easy to see that if $N > 1$, $b_{\text{app}} > b$. This conclusion offers a possible explanation of the discrepancy between the values of MBBA anchoring energy obtained experimentally in Blinov *et al.* [18]; homeotropic orientation by lecithin, anchoring energy 10^{-4} erg/cm^2; and in Barbero and Petrov [19], hometropic orientation by chromium distearyl chloride, anchoring energy $(10^{-3} - 10^{-2})$ erg/cm^2. Presumably, chromium distearyl chloride sticks to the surface stronger than lecithin and does not produce a sufficient surfactant gradient by desorption.

APPENDIX B: DYNAMIC SOLUTION

Theoretically, the in-phase component of $I(t)/I_0$ is

$$X = S\frac{\xi_S^2}{1+\left(1-\frac{\chi}{k_S}\xi_S\omega\right)^2}\left[\frac{d}{2}+\left(\frac{\chi}{k_s}\xi_S\omega-1\right)\left(\frac{d}{2}-\xi_S\right)\right]+B_2\xi_B^3+E_X, \quad \text{(B12)}$$

whereas the quadrature component is

$$Y = S\frac{\xi_S^2}{1+\left(1-\frac{\chi}{k_S}\xi_S\omega\right)^2}\left[\left(\frac{d}{2}-\xi_S\right)-\frac{d}{2}\left(\frac{\chi}{k_S}\xi_S\omega-1\right)\right] + B_2\xi_B^2(d-\xi_B-2\lambda)+E_y. \quad \text{(B13)}$$

The quantities E_X and E_Y are related to the exponential terms and are given by

$$E_X = e^{-\lambda/\xi_S}\frac{\xi_S^2}{1+\left(1-\frac{\chi}{k_S}\xi_S\omega\right)^2}\left[B_1\frac{\xi_B^2}{\xi_S^2}\left(p_1\cos\frac{\lambda}{\xi_S}+s_1\sin\frac{\lambda}{\xi_S}\right) - S\left(p_2\cos\frac{\lambda}{\xi_S}-s_2\sin\frac{\lambda}{\xi_S}\right)\right] \quad \text{(B14)}$$

and

$$E_Y = e^{-\lambda/\xi_S}\frac{\xi_S^2}{1+\left(1-\frac{\chi}{k_S}\xi_S\omega\right)^2}\left[B_1\frac{\xi_B^2}{\xi_S^2}\left(p_1\sin\frac{\lambda}{\xi_S}-s_1\cos\frac{\lambda}{\xi_S}\right) - S\left(p_2\sin\frac{\lambda}{\xi_S}+s_2\cos\frac{\lambda}{\xi_S}\right)\right], \quad \text{(B15)}$$

where the parameters $B_{1,2}$ and S are defined as

$$\begin{aligned} B_1 &= 2\frac{e_s}{e_B}C, \\ B_2 &= 2(1-e_S/e_B)c, \\ S &= 2\frac{\Delta n_S}{\Delta n_B}\left[\frac{e_s}{e_S}\frac{k_B}{k_S}\right]^2 \frac{1}{[1-(e_S/e_B-1)d/b/2]}c, \\ c &= \frac{1}{6}\left(\frac{\pi}{\lambda_0}\right)^2 \Delta n_B^2 \frac{e_B^4}{k_B^4} E_0^3 d^3 \left[\frac{1-(e_S/e_B-1)d/b/2}{1+d/b/2}\right]^3, \end{aligned} \tag{B16}$$

and

$$\begin{aligned} s_1 &= \left(1-\frac{\chi}{k_S}\xi_S\omega\right)\left(\frac{d}{2}-\lambda\right) - \left(\frac{d}{2}-\lambda-\xi_B\right), \\ p_1 &= \left(\frac{d}{2}-\lambda\right) + \left(1-\frac{\chi}{k_S}\xi_S\omega\right)\left(\frac{d}{2}-\lambda-\xi_B\right), \\ s_2 &= \left(1-\frac{\chi}{k_S}\xi_S\omega\right)\left(\frac{d}{2}-\lambda\right) + \left(\frac{d}{2}-\lambda-\xi_B\right), \\ p_2 &= \left(\frac{d}{2}-\lambda\right) - \left(1-\frac{\chi}{k_S}\xi_S\omega\right)\left(\frac{d}{2}-\lambda-\xi_B\right). \end{aligned} \tag{B17}$$

ξ_S and ξ_B are the penetration lengths defined in Equation (7).